Indian Journal of Pure & Applied Physics
Vol. 62, February 2024, pp. 116-123
DOI: 10.56042/ijpap.v62i2.7700

Effect of Multi-step Sintering on the density of $Li_7La_3Zr_{1.75}Ce_{0.25}O_{12}$ as Solid State Electrolyte Material

Sharad Singh Jadaun[a], Amrish K Panwar[a*] & Geetanjali[b]

[a]Department of Applied Physics, Delhi Technological University, Delhi 110 042, India
[b]Department of Chemistry, KMC, University of Delhi, Delhi 110 007, India

Received 31 December 2023; accepted 22 January 2024

The development of garnets structured lithium lanthanum zirconate, $Li_7La_3Zr_2O_{12}$ (LLZO) have many amicable characteristics such as high stability against lithium metal anode and wide electrochemical voltage window that make them good solid electrolytic materials for lithium-ion batteries. However, the poor interfacial properties and limited ionic conductivity continue to limit their wide range of applications. Hence, the current study has been focused on improving their ionic conductivity as well as the dense microstructure. This study demonstrates a simple and efficient method to produce compact ceramics with high Li^+ conductivity using a multi-step sintering process and variation in grain growth, relative density with the temperature and time variation has been studied. Therefore, garnet-structured oxides with the nominal chemical formula: $Li_7La_3Zr_{1.75}Ce_{0.25}O_{12}$ (LLZCO) have been synthesized. TGA, XRD and SEM characterization has been performed to see optimum calcination temperature, phase formation and microstructural analysis of the sample, respectively. The average crystallite size of the prepared LLZCO is estimated about 100 nm as calculated by Scherrer's formula from intense peaks of XRD pattern. Further, the ionic conductivity, electronic conductivities, activation energies along with the electrochemical voltage window stability have been explored.

Keywords: Solid state electrolyte; Solid state battery; LLZO; Lanthanide doping

1 Introduction

Lithium-ion batteries (LIBs) have a significant impact on the market as energy storage devices in today's information-rich world and are utilized as energy-storing devices for a variety of applications starting from light to heavy duty applications. In contrast to previous battery systems, LIBs have a high gravimetric energy density, long cycle life, and high volumetric energy density[1-2]. However, thermal instability, high flammability, and electrochemical instability of liquid electrolytes do have certain negative effects on lithium-ion batteries performance[2-3]. Moreover, the performance of liquid electrolytes is also limiting for high voltage cathode and lithium metal anode[1-4], lithium metal anodes in liquid electrolytes cause battery degradation owing to dendrite formation[5]. To overcome these challenges, solid-state electrolyte may be the potential alternative. As the solid state electrolytes are stable against high voltage cathode and lithium metal anode. They provide wide electrochemical voltage window for high energy LIBs.

An ideal solid electrolyte should possess good electrochemical stability, high ionic conductivity with low electronic conductivity and good mechanical stability[6-7]. Solid electrolyte with a garnet structure is a viable option for LIBs. Thangadurai *et al*. has developed garnet type Li oxides $Li_5La_3Nb_2O_{12}$ and $Li_5La_3Ta_2O_{12}$, with the room temperature ionic conductivity of about 10^{-6} Scm^{-1}[ref 8]. Murugan *et al*.[9] synthesized the $Li_7La_3Zr_2O_{12}$(LLZO) with high conductive cubic phase garnet structure than the less conductive tetragonal phase was synthesized by Awaka *et al*.[10]. Li-ion occupancy is the basic difference between these two structures, in which tetragonal garnet has three Lithium sites which occupy tetrahedral site (8a), octahedral site (16f) and octahedral site (32g). In cubic LLZO, Li occupies two types of sites as (24d) tetrahedral site and (96h) distorted octahedral site. Hence, for this cubic LLZO structure, Li-Li ion bond length is short which results in high ionic conductivity[11]. Despite of having high mechanical strength and high electrochemical voltage window, there are some of the major challenges for practical applications such as; (a) high electrode electrolyte interfacial resistance, (b) higher sintering temperature (c) lower ionic conductivity then liquid electrolyte.

To address the ionic conductivity issue, the doping in garnets with aliovalent ions (Al, Nb, Ta) is the

*Corresponding author: (E-mail: amrish.phy@dtu.ac.in)

most common method used to obtain the cubic lithium garnets with high conductivity. Lanthanides doping at La sites have been studied but it does not have any significant effect on the conductivity of garnets[12]. Ce doping on LLZO at La sites has been attempted, however, a limited incorporation of Ce was detected[13]. Doping with Ce on the site of Zr in LLZO is an effective method due to the large size of the Ce^{4+} ion in comparison to Zr^{4+} ion, as doping reduces the tetragonal distortion of LLZO resulting in high ionic conductivity of material[14].

Moreover, the high ionic conductivity can also be obtained by various sintering techniques like spark plasma sintering and hot press sintering in controlled sintering atmosphere *etc*[14]. Despite of optimizing these parameters, reaction mechanism during the sintering period is important to understand. It has been found that during sintering some impurity phase like $La_2Zr_2O_7$, $LiAlO_4$ creates hindrance in ionic movement, that can be eliminated at 1130 ºC for 12 hrs. Hence, the investigation reveals that sintering is also an important factor to consider[15, 16]. To minimize the impurity phase and increase the ionic conductivity of LLZO, Xu *et al.*[17] designed multi-step holding strategy to produce high density garnets.

Therefore, the present study demonstrates a simple and efficient method used to produce compact ceramics with high Li^+ ion conductivity using a multi-step sintering process to synthesize lithium garnet with molecular formula: $Li_7La_3Zr_{1.75}Ce_{0.25}O_{12}$ (LLZCO) as solid state electrolyte material. The structural, microstructural analysis, ionic conductivities, electronic conductivities and electrochemical voltage stability of the LLZCO are also studied and improved to support the electrochemical usages further.

2 Material and Methods

2.1 Material synthesis

Synthesis of LLZCO has been attempted via solid-state reaction route. All precursors Li_2CO_3, CeO_2, ZrO_2, La_2O_3 with purity >99% were dried in Metrex instrument make oven at 120 ºC overnight to remove any moisture present. In order to account for the lithium loss at high temperatures, 10% more Li_2CO_3 was added. Fig. 1 depicts a schematic of the synthesis of LLZCO. All the precursors were ball-milled in zirconia jar using ethanol as milling media to produce the raw powder, which was then calcined at 900 ºC in a box furnace for 10 hrs. The calcined powder was uniaxially pressed into pellets of diameter, 10 mm and thickness, 1.0 mm. These pellets were then moved to furnace for multi-step sintering process in which initially the pellet was sintered at 1150 ºC for 2 hrs than at 1100 ºC for 2, 4, 6, 8 hrs marked as sample T1, T2, T3, T4, respectively, in this study.

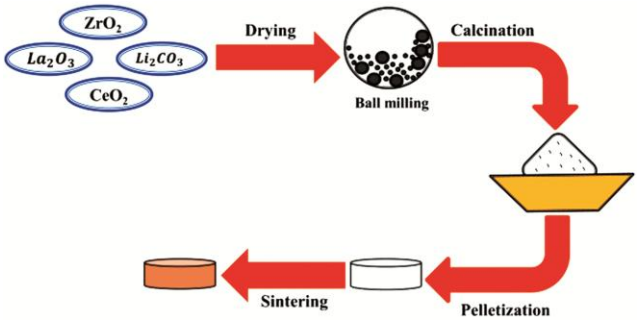

Fig. 1 — Schematic presentation of synthesis of LLZCO via solid state reaction route in ambient atmosphere.

2.2 Material characterization

As-synthesized sample was characterized by Thermogravimetric analysis (TGA) and Differential Scanning Calorimetry (DSC) to study the thermal stability and mass loss of the material via Perkin Elmer make model TGA 4000 equipment. Synthesized sample was characterized via X-ray diffractometer (Bruker make, model: D-8) using CuKα(λ=1.54Å) source in the range of 10-55° with a step size of 0.02°. Density of sintered pellets were calculated using simple physical process mass divided by volume. To study the microstructure of the sintered pellets using scanning electron microscopy (SEM), FEI make Nova Nano system has been used. The impedance spectroscopy analysis of LLZCO pellet has been carried out in the frequency range of 1 MHz to 4 Hz within the temperature range 30 and 70 °C using HIOKI make 3532 LCR meter. Hence, the estimation of ionic conductivity and activation energy were performed. Chronoamperometry test of dense pellet was done by biologic VMP3 potentiostat at a constant voltage of 100mV for 2 hrs to calculate its steady state electronic conductivity. Sintered pellet was coated by silver paste on both faces to make them electrically conductive. Electrochemical voltage stability was performed in the range of -0.5 V to 4.0 V using SS|LLZCO|Li cell, where stainless steel(SS) is used as working electrode and Li-metal as reference electrode. The cell fabrication was performed in MBraun make Ar filled Glove box workstation with O_2 and H_2O level less than 0.5 ppm.

3 Results and Discussion

3.1 Thermogravemetric(TGA) and differential scanning calorimetry(DSC) analysis

To study the phase formation and sintering temperature of LLZCO ball-milled product of the precursors was examined via TGA and DSC as shown in Fig. 2. TGA shows multi-stage mass loss occurs, initially 0.84% mass loss occurs that depicts the removal of moisture and reaction with La_2O_3 to form $La(OH)_3$. Further, mass loss of 2.01% and 2.25% accompanying with endothermic peaks (in DSC plot) at 335 and 450 °C can be attributed to La_2O_3 decomposition into LaOOH and then LaOOH reaction with CO_2, respectively[18]. Final mass loss of 17.44% starts from 700 °C, which indicate that the decomposition of Li_2CO_3 has been started leading to the formation of LLZCO[19]. It can be seen that above 1050 °C mass loss is negligible. Therefore, 1150 and 1100 °C has been considered for sintering temperature of material.

3.2 Structural analysis

X-ray diffraction analysis of an LLZCO sample sintered at 1150 °C for 2hrs is shown in Fig. 3 Stoichiometric amount of Ce doped $Li_7La_3Zr_2O_{12}$ can be indexed with cubic structure of space group: Ia-3d and it matched with standard JCPDS file: 01-080-6067. While extra peaks indicate the $La_{24}Ce_{12}Li_{24}O_{72}$ impurity phase[12]. The average crystallite size of LLZCO is calculated using Scherrer's formula which is given by Eq. 1. Fig. 4 shows the Williamson-Hall plot which is used to determine the micro-strain from the total peak broadening of diffraction peaks, using the expression stated in Eq. 2.

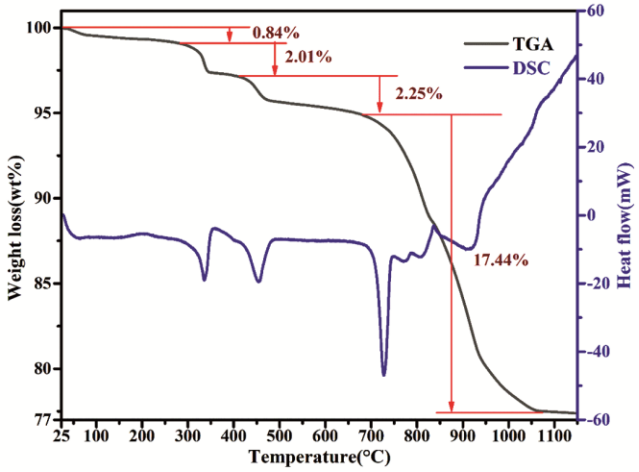

Fig. 2 — TGA/DSC curve of ball-milled product upto 1150 °C.

$$D = \frac{K\lambda}{\beta Cos\theta} \quad \ldots (1)$$

$$\beta_t = \frac{K\lambda}{DCos\theta} + 4\varepsilon tan\theta \quad \ldots (2)$$

Here, symbols β_t, β, λ, ε, D, and K are the total peak broadening, full width at half maxima, wavelength of X-ray source (1.54Å), micro-strain, crystallite size, and shape factor (0.9), respectively. High intense peaks in XRD are assigned to planes (211), (321), (400), (420), (422), (521), (611), (642) of LLZCO. The peaks are used to calculate the average full width at half maxima for crystallite size estimation. The micro-strain caused in the system is indicated by the slope of the fitted plot between 4sinθ and βcosθ. The average crystallite size calculated from Scherrer's formula is 100nm and micro-strain in crystal system obtained from the W-H plots is 3.55×10^{-4}, respectively. Smaller crystallite size is one of the reason for better sintering of a ceramic[20]. Here

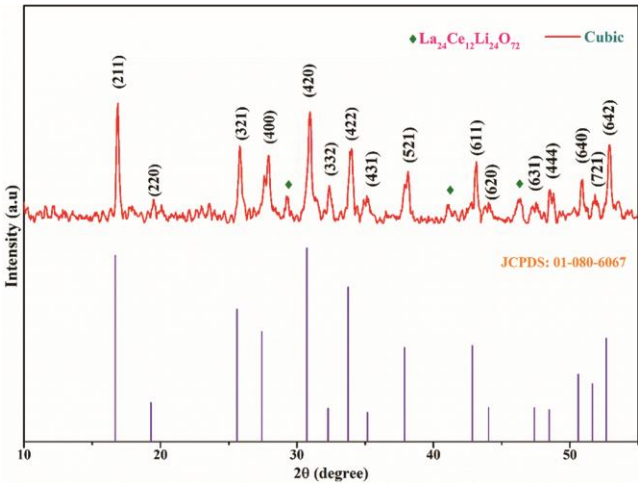

Fig. 3 — XRD pattern of LLZCO synthesized at 1150 °C for 2hrs.

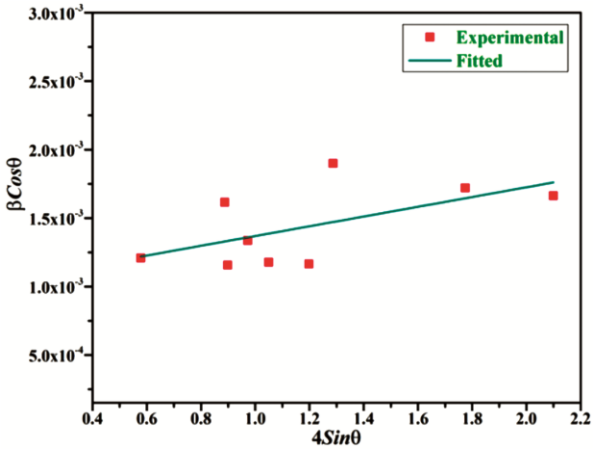

Fig. 4 — W-H plot of LLZCO sample.

in this study, it shows the sub-micron crystallite size range which is one of the reason for better sintering and lowering the sintering temperature of bare material[9].

3.3 Microstructure and density analysis

High density of the ceramic solid electrolyte is one of the major factor for the high conductivity and pure phase of the material. Therefore, LLZO pellet densification may prevent the growth of impurities. It is observed that at high temperature Al diffusion from alumina crucible can be diminished by higher relative density of the material which diminishes the impurity phase[16].

Fig. 5(a-d) display the SEM micrographs of LLZCO samplesT1, T2, T3 and T4 sintered initially at high temperature of 1150 °C for 2 hrs and then at 1100 °C for 2, 4, 6 and 8 hrs, respectively. The relative density results of these samples of material, LLZCO sintered at different schedules of temperatures and time are shown in Table 1. The difference in relative density of the material can be attributed to the grain growth and change in porosity of the material. Generally, in single step sintering from 900 °C to 1200 °C, grain size increases and porosity decreases which results in increment of relative density[16]. Among all the sintered samples, it can be analyzed that sample T2 reveals the highest relative density of 65%. The SEM images of different samples is shown in Fig. 5(a-d) which clearly shows that as the sintering time increases the grain boundary growth first increases and then decreases. Therefore, the increases/decrease in the density can be explained on the basis of movement of intergranular melt inside/outside of grains[17]. Fig. 5(b) shows that for sintering time of 4 hrs LLZCO showed interconnected and uniform grain distribution, which is in agreement with high relative density. The porosity increases as the exposure time increases more than 4 hrs as shown in Fig. 5(c-d). The higher sintering time may lead to lithium loss and reducing the grain size as uniform grain of sample T2 breaks into smaller flakes like grain for T3 and T4 samples. Fig. 6(a) shows the pellet before sintering and Fig. 6(b-e) show the sintered pellets of sample T1, T2, T3, T4, respectively. A reddish color in sample T4 pellet can be attributed to the lithium loss due to more sintering time. Fig. 6(f) shows the multiple production and reproducibility of density on 4-6 pellets of each sample. It can be seen that maximum density is

Table 1 — Multi-step sintering and Relative density of LLZCO samples.

S.no	Sample ID	Sintering Treatment	Relative Density
1.	T1	1150 °C for 2 hrs and 1100 °C for 2 hrs	44
2.	T2	1150 °C for 2 hrs and 1100 °C for 4 hrs	65
3.	T3	1150 °C for 2 hrs and 1100 °C for 6 hrs	61
4.	T4	1150 °C for 2 hrs and 1100 °C for 8 hrs	57

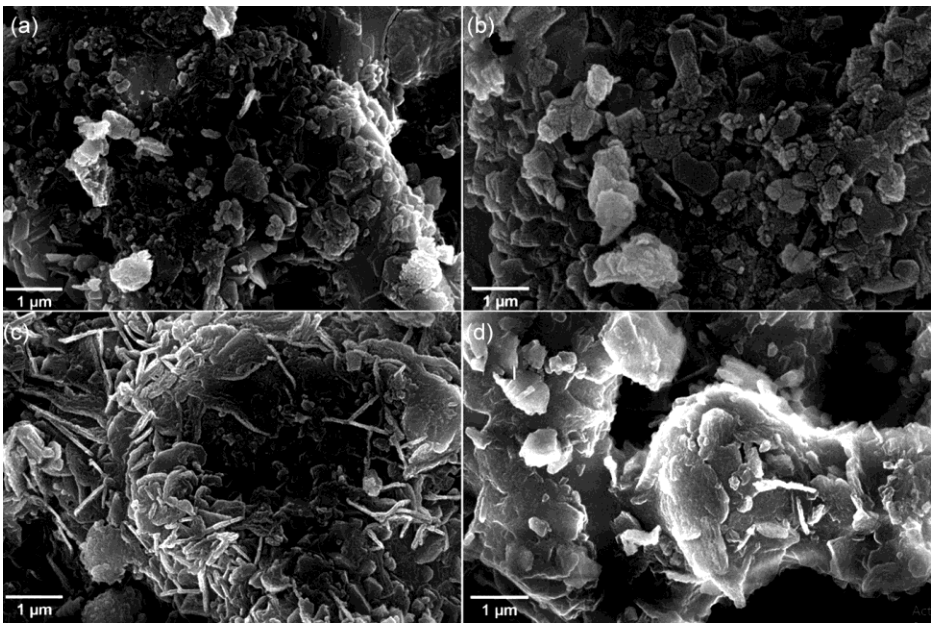

Fig. 5 — SEM micrograph of sample: (a)-T1, (b)-T2, (c)-T3 and (d)-T4 at a magnification of 25 KX.

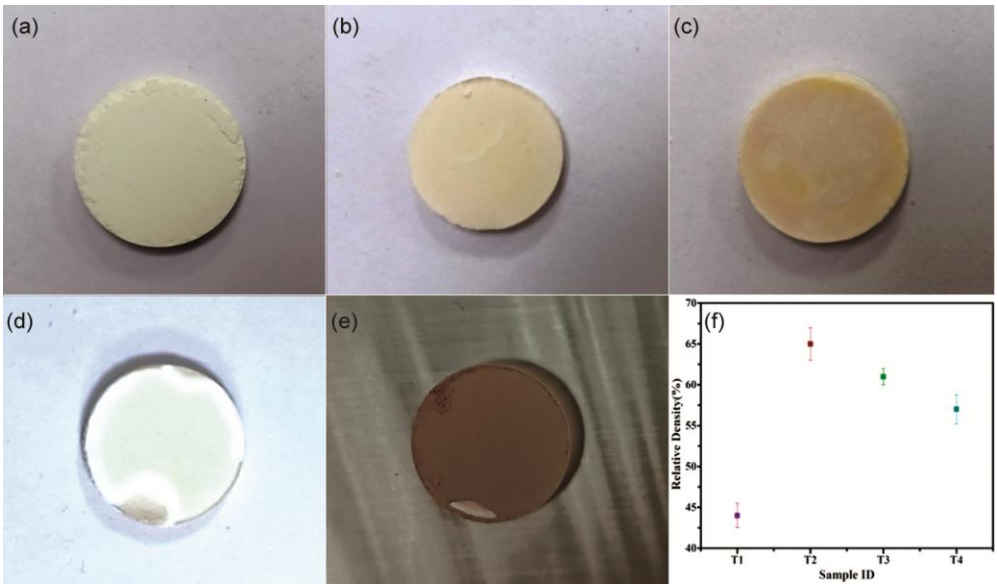

Fig. 6 — Before sintering (a); after sintering (b)T1, (c) T2, (d) T3, (e) T4, samples and (f)- variation of relative density in multiple attempts.

achieved for sample T2. SEM images of T2 sample is shown in Fig. 7, LLZCO pellets have the dense microstructure with average grain size of 408nm. Fig. 8(a-f) shows the elemental mapping of LLZCO which confirms almost homogeneous distribution of O, Zr, La, Ce, respectively, throughout the sample. The rise in intergranular melt with temperature is the cause of the increase in relative density, improved garnet phase and dense microstructure while multi-step sintering indicates the further densification of garnet at high temperature sintering[14].

3.4 Conductivity and activation energy analysis

Impedance spectroscopy measures sample's impedance over a broad frequency range and uses that information to characterize the material's various components based on their electrical relaxation times. Impedance is a combination of resistance, inductance and capacitance which can be calculated by passing AC signal through the sample[24]. Fig. 9 shows the impedance plot of Z' vs Z''pellet of LLZCO sample T2 sintered at 1150 °C for 2 hrs and then 1100 °C for 4hrs measured at 30 °C (room temperature). The semicircles observed in the high frequency region indicate the bulk and grain boundary contribution. Hence, each semicircle can be explained as equivalent to parallel combination of constant phase elements and resistance as shown in equivalent circuit of the inset of Fig. 9. Overall impedance is fitted via equivalent circuit of (R1)(R2Q1)(R3Q2)(Q3) using a EIS analyzer software, where R1, R2, R3 are electrode resistance, bulk resistance and grain boundary resistance respectively and Q1, Q2, Q3 are the constant phase elements. Hence, computed values for R1, R2, R3, Q1, Q2, Q3 are 2120 Ω, 7082 Ω,17050 Ω, 55.35×10^{-9} F, 2.11×10^{-9} F and 12.58×10^{-6} F, respectively, for impedance plot at room temperature. The ionic conductivity of the sintered pellets is calculated using the Eq. 3;

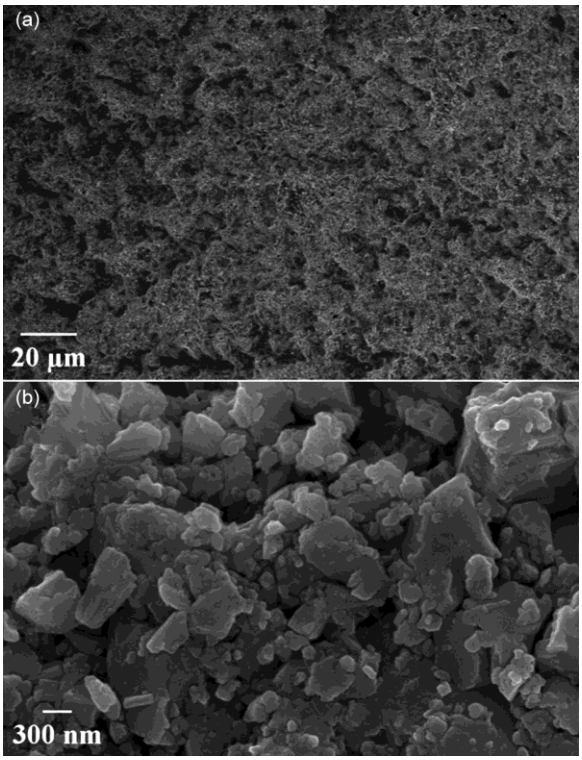

Fig. 7 — SEM micrograph of sample T2 pellet (a) 500 X (b) 45 KX.

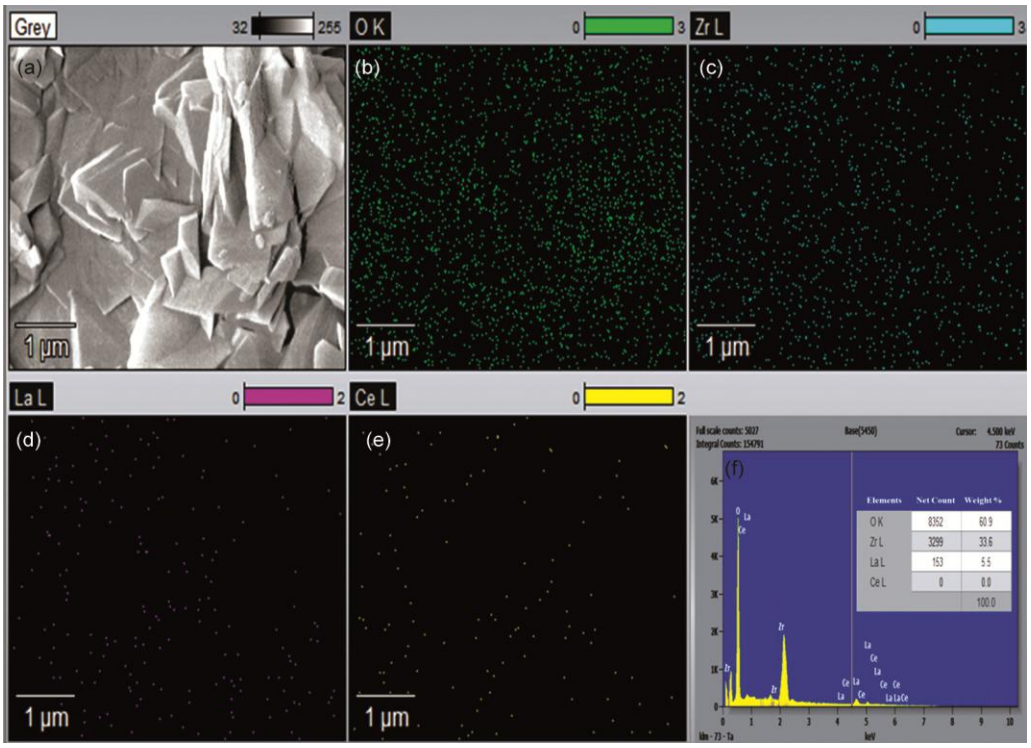

Fig. 8 — (a):SEM micrograph of sample T2; Elemental mapping images of (b)- O(green), (c)-Zr(blue), (d)- La(magenta), (e)- Ce(yellow) of LLZCO sample T2, (f) Result of EDS analysis of LLZCO.

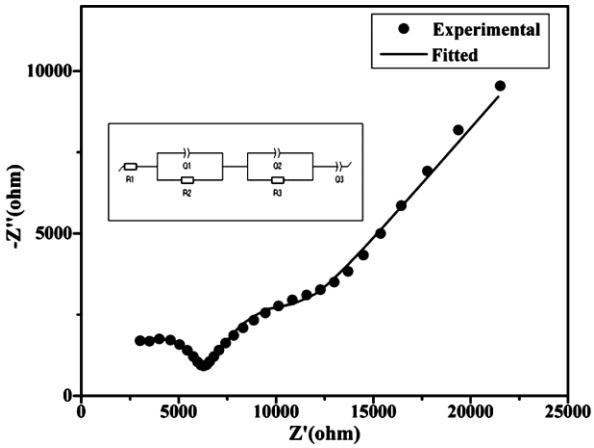

Fig. 9 — Z' Vs Z'' curveof LLZCO sample T2 pellet sintered at 1100 °C for 4 hrs at 30 °C.

$$\sigma = \frac{L}{R \times A} \quad \text{... (3)}$$

where R is the resistance of the sample in Ω, A is the area cm^2 and L is the thickness of the pellet in cm, respectively. The bulk ionic conductivity (σ) of the LLZCO material is observed as $0.17\times10^{-4}Scm^{-1}$ at 30 °C. Fig. 10 shows the impedance plots Z' vs Z'' at different higher temperatures ranging from 30 to 70 °C for sample T2. Here, it is observed that as the temperature increases both the contribution (bulk and grain boundary) merges. Therefore, the sum of the bulk and grain-boundary resistance contribution is considered for ionic conductivity calculation. Fig. 11 shows the temperature dependence of the conductivity estimated using Arrhenius Eq. 4 and given by;

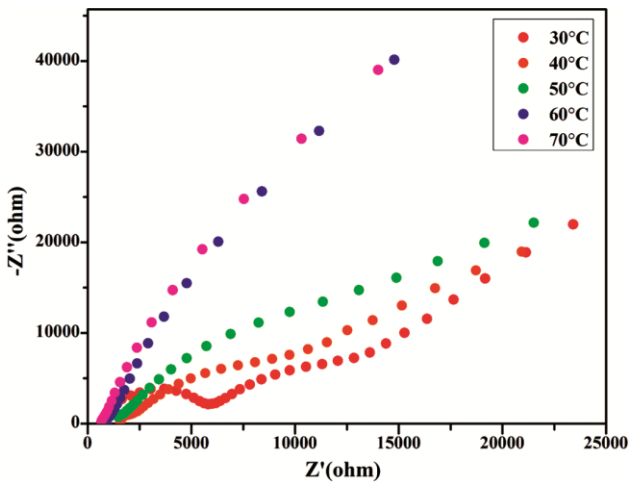

Fig. 10 — Temperature dependent impedance spectroscopy of LLZCO sample T2 pellet sintered at 1150 °C for 2 hrs and 1100 °C for 4 hrs from 30 °C to 70 °C.

$$\sigma = \sigma_0 e^{-E_a/K_B T} \quad \text{... (4)}$$

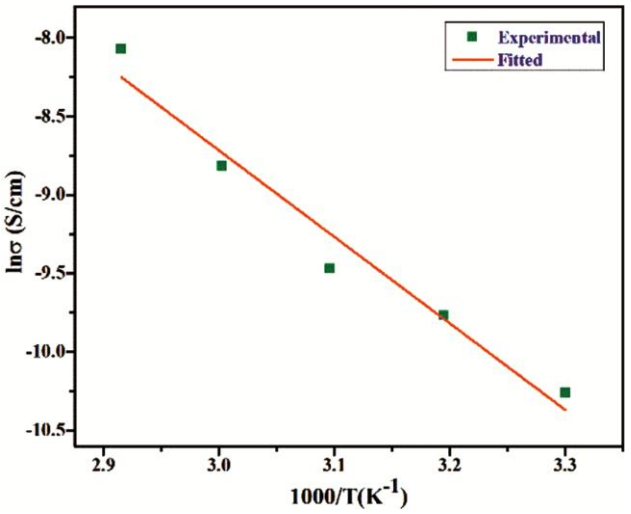

Fig. 11 — Activation energy curve of LLZCOsample T2 pellet sintered at 1150 ºC for 2 hrs and 1100 ºC for 4 hrs from 30 °C to 70 °C.

where σ, σ_o, E_a, T, K_B are ionic conductivity, pre-exponential factor, activation energy, temperature and Boltzmann constant, respectively. The activation energy was estimated to be 0.47 eV. Activation energy and ionic conductivity has a strong correlation between them as the activation energy decreases ionic conductivity increases while at the same time it has been seen that the Li^+diffusibility increases across the material due to lower in activation energy, high diffusibility of ions may enhance the cyclability of solid state battery[21]. Here, Ce stabilized LLZO activation energy(0.47 eV) value can be seen as of the decrease in activation energy from bare LLZO[10]. Fig. 12 shows the chronoamperometry curve of LLZCO pellet which is used to calculate the electronic conductivity of solid electrolyte using Eq. 5;

$$\sigma_e = \frac{I_{SS} \times L}{V \times A} \quad \ldots (5)$$

Where σ_e, I_{SS}, I_o, L, V, A are electronic conductivity, steady state current, thickness of pellet, polarization voltage, area of pellet, respectively[22]. It can be seen that the value of initial output current (I_o) of LLZCO sample is 2.33×10^{-5} mA, after two hours of constant voltage input sample shows very low value of steady state current (ISS), 5.24×10^{-6} mA, it leads to the negligible electronic conductivity (σ_e), 1.00×10^{-8}Scm^{-1} of LLZCO ceramic solid state electrolyte. Lower values of σ_e is very crucial for battery application as high electronic conductivity, σ_e favour the dendrite formation in Li^+ batteries which results in short circuiting of battery, decrease in coulombic efficiency

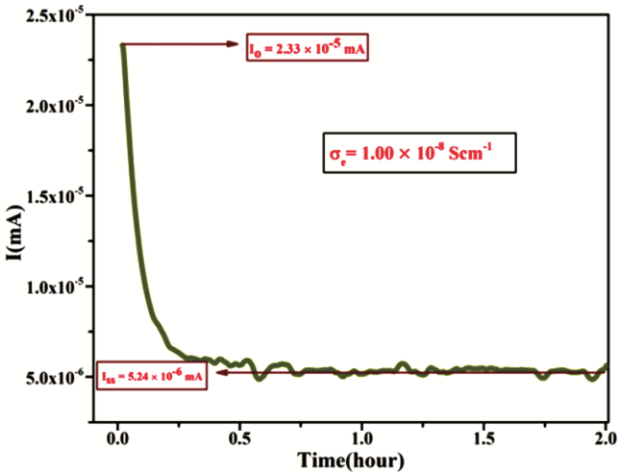

Fig. 12 — Chronoamperometry of LLZCO(T2) pellet sintered at 1150 °C for 2 hrs and 1100 °C for 4 hrs.

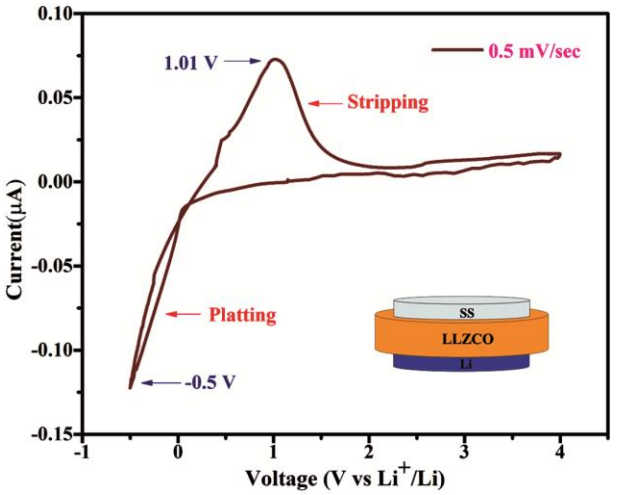

Fig. 13 — Cyclic Voltammetry analysis of LLZCO sample T2 pellet sintered at 1150 °C for 2 hrs and 1100 °C for 4 hrs solid electrolyte in the range of -0.5 V to 4 V.

and capacity loss[23]. Ce doping in LLZO is helpful to stabilize cubic phase at lower temperature as compared to undoped LLZO[9]. Hence, multi-step sintering approach leads to the formation of dense ceramic and yields high conductivity then undoped LLZO tetragonal phase. These alterations are beneficial for solid electrolyte application[10].

3.5 Electrochemical Analysis

The cyclic voltammetry (CV) analysis of LLZCO of sample T2 has been attempted to test the electrochemical stability using SS|LLZCO|Li cell configuration. Here, Stainless Steel (SS) is used as working electrode and Li metal chip is used as reference electrode. Fig. 13 shows the CV curve ranging from -0.5 to 4.0 V at a scan rate of 0.5 mV/s.

The peaks observed at -0.5 V and 1.01 V corresponds to Li platting and stripping, respectively. The broadening of peaks can be attributed to additional redox process taken place due to cerium, Ce_4O_7 phase formation and because of reaction at the interface or insertion of excessive Li in the electrolyte structure[14]. Furthermore, curve shows that there is no other extra oxidation peak upto 4.0 V which indicates that LLZCO has wide and stable electrochemical window to lithium metal and can be used for high energy density Li-ion batteries applications.

4 Conclusion

In this study, a garnet type $Li_7La_3Zr_2O_{12}$ is successfully synthesized via solid state reaction route. TGA/DSC analysis has been carried out upto 1150 °C to check the mass loss and optimum temperature range for multi-step sintering.TGA shows overall 22% mass loss has been occurred till 1050 °C and exothermic peak above 950 °C shows the crystallization has been started. Hence, 1150 and 1100 °C temperatures has been used for multi-step sintering. XRD analysis confirms that LLZCO has a garnet-type structure (space group: Ia-3d) with some impurities of the $La_{24}Ce_{12}Li_{24}O_{72}$. High temperature sintering at 1150 °C for 2 hrs followed by 1100 °C for 4 hrs shows the highest relative density, dense microstructure and uniform grain distribution of synthesized LLZCO solid state electrolyte. The bulk Li-ion conductivity (σ) of as synthesized LLZCO solid electrolyte is observed, $0.17\times10^{-4}Scm^{-1}$ along with low electronic conductivity (σ_e) of $1.00\times10^{-8}Scm^{-1}$. Minimum activation energy of the optimized sample T2 of LLZCO is observed as 0.47 eV. Electrochemical analysis by CV result shows platting peaks of lithium ion at -0.5 V and broad stripping peak for lithium ion is due to Ce_4O_7 phase formation. Hence, no other peak has been detected upto 4 V in CV plot, hence the electrolyte is stable upto 4.0 V.

Acknowledgment

Authors acknowledge Delhi Technological University, Delhi to provide financial support through a project grant “DTU/IRD/619/2019/2114” to carry this research work.

References

1 Larcher D & Tarascon J M, *Nature Chem*, 20 (2018) 19.
2 Mrinalini M, Hsu C, Rath P C, Patra J, Lai H Z, Chang T L, Wang C, Wu T, Lee T & Chang J, *Electrochimica Acta*, 353 (2020) 136536.
3 Lebedeva N P & Boon L, *J Electrochem Soc*, 163 (2016) A821.
4 Wu B, Wang S, Lochala J, Desrochers D, Liu B, Zhang W, Yang J & Xiao J, *Energy Environ Sci*, 11 (2018) 1803.
5 Liu B, Zhang J & Xu W, *Joule*, 2 (2018) 833.
6 Samson A J, Hofstetter K, Bag S & Thangadurai V, *Energy Environ Sci*, 12 (2019) 2957.
7 Meesala Y, Jena A, Chang H & Liu R, *ACS Energy Lett*, 2 (2017) 2734.
8 Thangadurai V, Kaack H & Weppner W J F, *J Am Ceram Soc*, 86 (2003) 437.
9 Murugan R,Thangadurai V & Weppner W, *Angewandte Chem Int Edn*, 46 (2007) 7778.
10 Awaka J, Kijima N, Hayakawa H & Akimoto J, *J Solid State Chem*, 182 (2009) 2046.
11 Jiang C, Li H & Wang C, *Sci Bull*, 62 (2017) 1473.
12 Abin K, Seungjun W, Minseok K, Heetaek P & Byoungwoo K, *Front Chem*, 8 (2008).
13 R Ezhiylmurugan, W Jeff, A Jan & S Jeff, *J Power Source*, 230 (2013) 261.
14 Dong B, Yeandel S R, Goddard P & Slater P R, *Chem Mater*, 32 (2019) 215.
15 Henrik B, Janis D, Stefan B, Alexander K, Patrick B, Martin W, Paul H, Anatoliy S, Helmut E, Andriy L, Viola D, Lorenz K & Jürgen J, *Phys Chem Chem Phys*, 13 (2011) 19378.
16 Xia W, Xu B, Duan H, Guo Y, Kang H, Li Hua & Liu Hezhou, *ACS Appl Mater Interfaces*, 8 (2016) 5335.
17 Xu B, Duan H, Xia W, Guo Y, Kang H, Li H & Liu H, *J Power Source*, 302 (2016) 291.
18 Janez K, Seyedabolfazl M, Benjamin W, Eeva-Leena R & Tanja K, *Solid State Ionics* 380 (2022) 115943.
19 Marlou K, Battista A G, Guk-Tae K, Varvara S, Meike S, Jörg S, Andreas R & Stefanoi P, *J Power Source*, 353 (2017) 287.
20 Andrew R & Ian C, *Metal-Reinforced Ceram*, (2021) 211.
21 Manju S & Yashonath S, *The J Chem Phys*, 129 (2008) 144103.
22 Ramasubramonian D & Reza S, *Batteries Supercaps*, 4 (2021) 596.
23 Fudong H, Andrew W S, Jie F, Fei W, Miaofang C, Donovan L, Nancy D, Howard W & Chunsheng W, *Nature Energy*, 4 (2019) 187.
24 Brugge, Rowena, *Garnet ceramic electrolytes for next-generation lithium batteries*, University of London, 2018.